



RESEARCH ARTICLE

# Dynamic modeling and characterization of compliant cable-driven parallel robots containing flexible cables

Miaojiao Peng<sup>1,2</sup> , Longhai Xiao<sup>1,2</sup>, Qinglin Chen<sup>1,2</sup>, Guowu Wei<sup>3</sup> , Qi Lin<sup>4</sup> and Jiayong Zhuo<sup>1,2</sup>

<sup>1</sup>School of Marine Engineering, Jimei University, Xiamen, China, <sup>2</sup>The Key Laboratory of Ship and Marine Engineering of Fujian Province, Xiamen, China, <sup>3</sup>School of Computing, Science & Engineering, University of Salford, Salford, UK, and <sup>4</sup>School of Aerospace Engineering, Xiamen University, Xiamen, China

**Corresponding author:** Qinglin Chen; Email: [cql@jmu.edu.cn](mailto:cql@jmu.edu.cn)

**Received:** 9 February 2022; **Revised:** 12 April 2023; **Accepted:** 14 June 2023; **First published online:** 28 July 2023

**Keywords:** cable-driven parallel robot; cable vibration; nonlinear dynamics; parallel manipulators; compliant robots

## Abstract

Flexible cables in cable-driven parallel robots (CDPRs) are easy to be excited and vibrate. Cable vibration will react on the end-effector, causing attitude deviation of the end-effector. The main objective of this study is to accurately model axially moving flexible cables and characterize the dynamic behaviors of associated compliant CDPRs. Firstly, a model for transverse vibration of the axially moving length-variable cable is developed. On this basis, an original nonlinear dynamic model of the CDPRs able to capture the vibration of the cables and the dynamics of the end-effector is proposed. Secondly, the frequency–amplitude relationship of the CDPR is obtained. Moreover, the significance of the excitation effect caused by the axially moving length-variable cables is demonstrated, by comparing the results with and without excitation effect at different frequencies. It turns out that, as the oscillation frequency of the end-effector increases, the end-effector and cables exhibit the dynamics process from steady state to unstable large-amplitude vibration and finally to stable small-amplitude vibration. This indicates that the dynamics of the CDPR exhibit non-linear characteristics, due to the influence of flexible cables. Finally, the proposed dynamic model of compliant CDPRs is validated by experiments performed in the laboratory.

## 1. Introduction

Cable-driven parallel robots (called CDPRs for short throughout the paper) are a new type of mechanisms based on parallel robot technology [1]. A CDPR is formed by a base, an end-effector, a number of driving cables, and motion control units. The motion control of the end-effector is performed by modifying the lengths of the cables [2]. CDPRs have the advantages of large workspace, light weight, high load capacity, fast response, and easy reconfiguration. As a result, they are widely used in the fields of the aerial panoramic photographing [3, 4], the medical rehabilitation [5, 6], the wind tunnel test [7–10], the radio telescope [11], and so on.

Because of the flexibility of cables, the vibration of CDPRs becomes a vital concern. Vibrations of CDPRs can be induced by (brutal) end-effector velocity changes, wind disturbance, and/or speed reducer backlash [12, 13]. Vibrations of CDPRs mainly include vibrations of the cables and the end-effector. Vibrations of CDPRs can affect the static and dynamic behaviors of CDPRs, such as the positioning accuracy, trajectory tracking, as well as the force distribution and control [12–15]. In applications requiring high positioning precision, high system stiffness, and/or high dynamic performances, vibrations of CDPRs are an important issue [13, 16]. Moreover, the oscillation of the end-effector may cause vibration in the cables. The vibrating cables may react on the end-effector and cause large-amplitude vibration of the end-effector [13]. When large-amplitude vibrations of CDPRs occur, even serious damage to the

CDPRs may happen. Hence, a detailed study of cable vibration and the resulting dynamic responses of CDPRs is desired.

Studies of CDPRs are mostly focus on force distribution [17–19], workspace analysis [20, 21], trajectory planning [22, 23], and motion control [24, 25]. Only a few studies are dedicated to the vibration analysis of CDPRs [12–14, 26, 27]. In ref. [12], a dynamic stiffness analysis of CDPRs based on the dynamic stiffness matrix method is presented, and the modal interaction is analyzed. In ref. [13], the dynamic model for cable-driven parallel manipulators is achieved considering the relationship between the motion of the end-effector and the cable end force. In ref. [14], a new approach is proposed to compensate the rotational oscillations of the end-effector, using reaction wheels. In ref. [26], a model relating the motion of the end-effector and the cable tension is provided to investigate the trajectory tracking of the end-effector. In ref. [27], the effect of the cable vibration on the natural frequencies of the cable-driven parallel manipulator is analyzed. However, few studies consider the cable vibration and its effect on the motion of the end-effector in CDPRs.

Cable vibration is a key problem in the dynamic analysis of CDPRs. Research on the cable vibration mostly can be found in the engineering fields such as cable-stayed bridges and power transmission lines [28–30]. In the modeling of cable vibration, Tagata [31] reduces the cable to a massless tensioned string and derives the dimensionless Mathieu equation. On this basis, many scholars have done a lot of research on the parametric vibration of cables [32–35]. However, in the above studies, the cable is stationary along its axial direction and the cable length is invariable.

For the vibration of an axially moving string, an axially moving string/cable may undergo transverse vibration excited by its axial acceleration. A small excitation can produce a large response in such parametrically excited systems [36, 37]. Mote [38] first studied the parametric vibration of an axially moving string due to the variation in tension using a modal analysis. Ghayesh [39, 40] investigated the parametric vibration and stability of an axially accelerating string, assuming a mean axial velocity with small harmonic fluctuations. Yurddaş *et al.* [41, 42] studied the nonlinear vibration of axially moving strings under non-ideal support. The nonlinear equations of motion and boundary conditions were derived using Hamilton's principle, and the axial motion was modeled using harmonic variable velocity functions. Similarly, the governing equation of motion describing the transverse vibrations of the axially moving string is derived from Hamilton's principle in refs. [36, 43].

However, in the above studies, although the excitation of periodically fluctuating tension and velocity on the cable is considered, the excitation effect of time-varying length is not considered. Moreover, the boundary condition of the cable is that both ends are constrained, which is very different from the CDPRs. For the CDPRs in this study, one end of the cable moves spatially along with the end-effector. Further study is needed to be dedicated to the vibration of the axially moving cable excited by its periodically fluctuating tension and velocity along with the time-varying length. Therefore, it is essential to set up a brand new model to investigate the dynamic behavior of CDPRs containing axially moving flexible cables of time-varying length. Moreover, an effective model can provide a useful tool for the dynamic analysis of CDPRs. Research on the dynamic behavior of CDPRs can provide constructive guidelines for the design and optimization of CDPRs.

This study is organized as follows. In Section 2, the problem of dynamic relationship between the end-effector and the cables of CDPRs is illustrated. In Section 3, an original nonlinear dynamic model of CDPRs able to capture the vibration of the cables and the dynamics of the end-effector is established. An implicit numerical integration algorithm is used to solve the nonlinear partial differential equation of CDPRs. In Section 4, based upon the proposed model of a 6-degree of freedom (DOF) 8-cable CDPR, the frequency–amplitude relationship of the CDPR is obtained. And the significance of the excitation effect caused by the axially moving length-variable cables is demonstrated by comparing the results with and without excitation effect at different frequencies. In Section 5, dynamic experiments are performed in the laboratory to validate the proposed dynamic model of compliant CDPRs. In Section 6, concluding remarks are finally given.

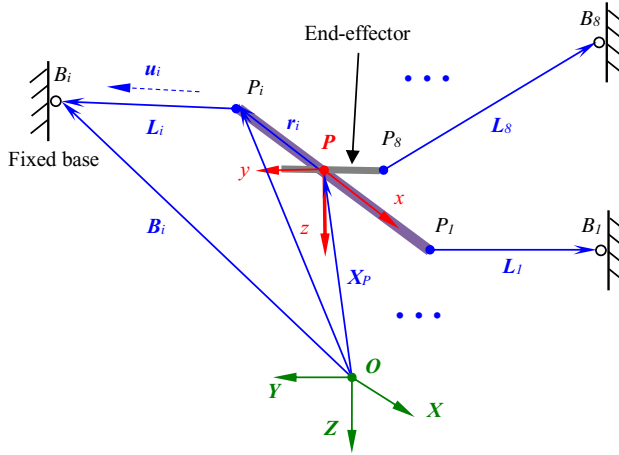


Figure 1. Kinematics schematic of a 6-DOF 8-cable CDRP.

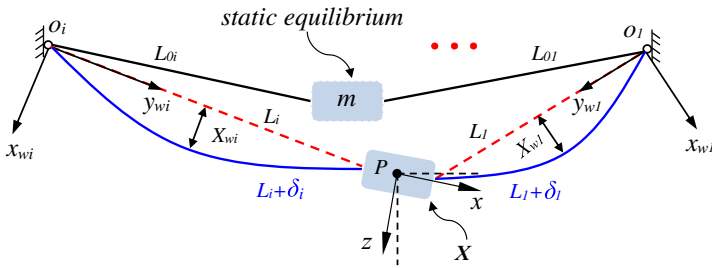


Figure 2. A simplified dynamic model of a 6-DOF CDRP.

2. Problem descriptions

A 6-DOF 8-cable CDRP is illustrated in Fig. 1. The purpose of using eight cables is to enable the cables in tension during operation [27] and make the structure layout symmetrical. The number of cables can be seven or more than seven in the design. The end-effector is suspended in the air by eight cables. The 6-DOF motion of the end-effector can be controlled by changing the length of the driving cables. As shown in Fig. 1, a global frame  $OXYZ$  and a local frame  $Pxyz$  are set up. The origin of the local frame  $Pxyz$  is set at the mass center of the end-effector (point  $P$ ).  $B_i (i = 1, 2, \dots, 8)$  is the contact point between the cable and the pulley;  $P_i (i = 1, 2, \dots, 8)$  is the anchoring point of the cable with the end-effector; and  $u_i (i = 1, 2, \dots, 8)$  is the direction vector for the  $i$ th cable.

A simplified dynamic model of a 6-DOF CDRP is shown in Fig. 2. For convenience, one end of each cable is assumed to be fixed, with the other end attached to the end-effector. Initially, the end-effector is at the static equilibrium, and the cables are in a tension state with the initial length  $L_{0i}$ . When the end-effector performs an oscillating motion, the cables will accelerate axially and the lengths of the cables will alter accordingly. This axial acceleration may excite the cables, resulting in vibration of the cables. Besides, the vibrating cables will react on the end-effector. The instantaneous attitude of the end-effector is  $X = [X_p, Y_p, Z_p, \phi, \theta, \psi]^T$ , which characterize the three translations ( $X_p, Y_p, Z_p$ ) and the three rotations ( $\phi, \theta, \psi$ ). The instantaneous length of the cable during the motion of the end-effector is  $L_i$ , and the elastic extension in the cable caused by the vibration of the cable is  $\delta_i$ .

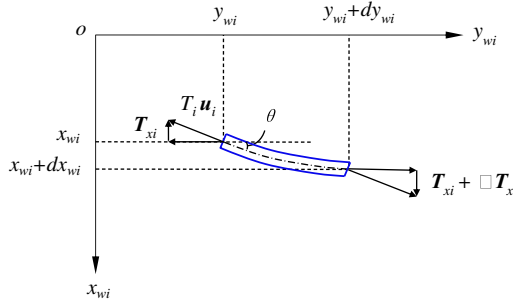


Figure 3. Force analysis of the differential cable element.

### 3. Problem formulations

#### 3.1. Dynamics of the end-effector

In global frame  $OXYZ$ , the length vector of the  $i$ th cable  $L_i$  is defined as [44]:

$$L_i = B_i - X_P - R x_{P_i} \tag{1}$$

where  $B_i = \overrightarrow{OB_i}$ ,  $X_P = \overrightarrow{OP} = [X_P, Y_P, Z_P]^T$  represents the position vector of point  $P$  in global frame  $OXYZ$ ;  $x_{P_i}$  is the position vector of point  $P_i$  in local frame  $Pxyz$ ; and  $R$  is the transformation matrix from  $Pxyz$  to  $OXYZ$ .

As shown in Fig. 1, the end-effector is considered as a rigid body, and the equation of motion for the end-effector can be established based on the Newton–Euler method [44]:

$$M \ddot{X} + W_C - W_G = J_A^T T \tag{2}$$

where  $M = \begin{bmatrix} (mI)_{3 \times 3} & \mathbf{0}_{3 \times 3} \\ \mathbf{0}_{3 \times 3} & A_G H \end{bmatrix}$  denotes the mass matrix;  $H = \begin{bmatrix} \cos \theta \cos \psi & -\sin \psi & 0 \\ \cos \theta \sin \psi & \cos \psi & 0 \\ -\sin \theta & 0 & 1 \end{bmatrix}$ ;  $m$  is the mass of the end-effector;  $A_G$  is the inertia matrix of the end-effector about its mass center (point  $P$ ).  $W_C$  denotes the nonlinear Coriolis force,  $W_G$  denotes the gravity vector of the end-effector, and  $J_A^T$  denotes the Jacobian matrix of the CDP.  $T$  is the tension vector,  $T = [T_1, T_2, \dots, T_8]^T$ , and  $T_i (i = 1, 2, \dots, 8)$  represents the tension in the  $i$ th cable. The calculation expressions for the above variables can be found in ref. [44].

#### 3.2. Modeling of the cable

It is assumed that the cables are homogeneous. The cables are always in a tension state with the diameter  $d \leq 3$  mm. Therefore, the cables' gravity is not taken into account. The bending stiffness of the cables is negligible, because the cables can sustain only tensile forces. Considering the elastic effect of the cables, the deformation of the cables conforms to Hooke's law.

Consider the transverse vibration of the cable, since the sag of the cable is close to zero [45]. Taking one cable as an example, as shown in Fig. 3, force analysis of the differential cable element is carried out. The axial direction is along  $oy_{wi}$ , and the transverse direction is along  $ox_{wi}$ . An approximation  $ds_i \approx dy_{wi}$  is made for the differential cable element. The cable tension is  $T_i u_i$ , and  $u_i$  is the unit directional vector of cable tension for the  $i$ th cable. The transverse component of the cable tension is  $T_{xi}$ ,  $|T_{xi}| \approx -T_i \frac{\partial x_{wi}}{\partial y_{wi}}$ , and  $|T_{xi} + \Delta T_{xi}| \approx T_i \frac{\partial x_{wi}}{\partial y_{wi}} + T_i \frac{\partial}{\partial y_{wi}} \frac{\partial x_{wi}}{\partial y_{wi}} dy_{wi}$ . The transverse motion equation of the  $i$ th cable can be obtained from the balance of forces:

$$\rho_w A ds_i \dot{v}_{xi} = T_i \frac{\partial^2 x_{wi}}{\partial y_{wi}^2} dy_{wi} + F_{xi} \tag{3}$$

where  $\rho_w$  is the cable’s density,  $A$  is the cross-sectional area of the unstrained cable,  $ds_i$  is the arc length of the differential cable element,  $v_{xi}$  is the velocity in the direction of  $ox_{wi}$ ,  $\dot{v}_{xi}$  is the acceleration in the direction of  $ox_{wi}$ , and  $F_{xi}$  is the external force in the direction of  $ox_{wi}$ .

The axial speed of the  $i$ th cable (in the direction of  $oy_{wi}$ ), denoted by  $v_{yi}(t)$ , is time dependent. At axial coordinate  $y_{wi}$  and time  $t$ , the transverse vibration of the cable is specified by the transverse displacement  $x_{wi}(y_{wi}, t)$  [36]. So  $v_{xi} = \frac{dx_{wi}}{dt}$ . Then

$$\begin{aligned} \dot{v}_{xi} &= \frac{\partial}{\partial t} \left( \frac{dx_{wi}}{dt} \right) + \frac{\partial}{\partial y_{wi}} \left( \frac{dx_{wi}}{dt} \right) \frac{dy_{wi}}{dt} \\ &= \frac{\partial^2 x_{wi}}{\partial t^2} + 2v_{yi} \frac{\partial^2 x_{wi}}{\partial y_{wi} \partial t} + \dot{v}_{yi} \frac{\partial x_{wi}}{\partial y_{wi}} + v_{yi}^2 \frac{\partial^2 x_{wi}}{\partial y_{wi}^2} \end{aligned} \tag{4}$$

Consider the approximation of  $ds_i \approx dy_{wi}$ . Suppose the external force  $F_{xi}$  is zero. By substituting Eq. (4) into Eq. (3), the partial differential equation for the transverse displacement of the  $i$ th cable can be derived [36]:

$$\rho_w A \left( \frac{\partial^2 x_{wi}}{\partial t^2} + 2v_{yi} \frac{\partial^2 x_{wi}}{\partial y_{wi} \partial t} + \dot{v}_{yi} \frac{\partial x_{wi}}{\partial y_{wi}} + v_{yi}^2 \frac{\partial^2 x_{wi}}{\partial y_{wi}^2} \right) = T_i \frac{\partial^2 x_{wi}}{\partial y_{wi}^2} \tag{5}$$

To obtain the numerical solution of Eq. (5), the Galerkin method is applied to discretize the spatial variable. Then the solution of Eq. (5) can be expressed as:

$$x_{wi} = X_{wi} \sin \left( \frac{\pi y_{wi}}{L_i} \right) \tag{6}$$

where  $X_{wi}$  is the function of time  $t$ ,  $y_{wi} \in [0, L_i]$ .

Substituting Eq. (6) into Eq. (5) gives

$$\begin{aligned} \rho_w A \left( \sin \left( \frac{\pi y_{wi}}{L_i} \right) \ddot{X}_{wi} + 2v_{yi} \left( \frac{\pi}{L_i} \right) \cos \left( \frac{\pi y_{wi}}{L_i} \right) \dot{X}_{wi} + \dot{v}_{yi} \left( \frac{\pi}{L_i} \right) \cos \left( \frac{\pi y_{wi}}{L_i} \right) X_{wi} - v_{yi}^2 \left( \frac{\pi}{L_i} \right)^2 \sin \left( \frac{\pi y_{wi}}{L_i} \right) X_{wi} \right) \\ + T \left( \frac{\pi}{L_i} \right)^2 \sin \left( \frac{\pi y_{wi}}{L_i} \right) X_{wi} = 0 \end{aligned} \tag{7}$$

Setting  $y_{wi} = \frac{L_i}{2}$ , the transverse vibration equation for the mid-span of the  $i$ th cable can be obtained:

$$\ddot{X}_{wi} - \left( \frac{\pi}{L_i} \right)^2 \left( v_{yi}^2 - \frac{T_i}{\rho A} \right) X_{wi} = 0 \tag{8}$$

where the axial velocity of the cable  $v_{yi}$  is related to the motion of the end-effector, and the cable tension  $T_i$  is related to the motion of the end-effector and the cable vibration. The expression of these two variables is needed to be established to get the complete vibration equation of the cable.

### 3.2.1. Expression of $v_{yi}$

Based on Eq. (1), each side of it can be double as:

$$L_i^2 = (\mathbf{X}_p + \mathbf{R}\mathbf{x}_{p_i} - \mathbf{B}_i)^T (\mathbf{X}_p + \mathbf{R}\mathbf{x}_{p_i} - \mathbf{B}_i) \tag{9}$$

Taking derivatives of both sides of Eq. (9) with respect to time  $t$  gives

$$L_i \dot{L}_i = (\mathbf{L}_i)^T (\dot{\mathbf{X}}_p + \dot{\mathbf{R}}\mathbf{x}_{p_i}) \tag{10}$$

Taking derivatives of the transformation matrix  $\mathbf{R}$  with respect to time  $t$  gives

$$\dot{\mathbf{R}} = \mathbf{R}^\circ \mathbf{R} \tag{11}$$

where  $R^\circ = \begin{bmatrix} 0 & -\omega_Z & \omega_Y \\ \omega_Z & 0 & -\omega_X \\ -\omega_Y & \omega_X & 0 \end{bmatrix}$ ,  $\omega$  is the angular velocity vector of the end-effector, and  $\omega = H[\dot{\phi}, \dot{\theta}, \dot{\psi}]^T = [\omega_X, \omega_Y, \omega_Z]^T$ .

Substituting Eq. (11) into Eq. (10) gives

$$L_i \dot{L}_i = (L_i)^T \dot{X}_p + (r_i \times L_i)^T \omega \tag{12}$$

The expression of the axial velocity of the  $i$ th cable can be derived from Eq. (12):

$$v_{yi} = \dot{L}_i = u_i^T \dot{X}_p + (r_i \times u_i)^T \omega \tag{13}$$

### 3.2.2. Expression of $T_i$

The total tension  $T_i$  of the  $i$ th cable consists of three components: (1) the initial tension  $T_{0i}$ , (2) the variation of the cable tension  $T_{ei}$  caused by the 6-DOF motion of the end-effector, and (3) the variation of the cable tension  $T_{\delta i}$  caused by the vibration of the cable.

Using the definitions of  $L_{0i}$  and  $L_i$  listed in Section 2, the boundary elongation  $\Delta L_i$  caused by the motion of the end-effector can be described as:

$$\Delta L_i = L_i - L_{0i} = \sqrt{(B_i - X_p - R x_{p_i})^T (B_i - X_p - R x_{p_i})} - L_{0i} \tag{14}$$

Due to  $\partial x_{wi} / \partial y_{wi} \ll 1$  in the vibration of the cable that is in tension tightly, from Eq. (6) with an approximation made, the extension  $\delta_i$  in the elastic deformation caused by the vibration of the  $i$ th cable can be derived:

$$\begin{aligned} \delta_i &= \int (ds_i - dy_{wi}) = \int_0^{L_i} \left\{ dy_{wi} [1 + (\partial x_{wi} / \partial y_{wi})^2]^{1/2} - dy_{wi} \right\} \\ &\approx \int_0^{L_i} \frac{1}{2} (\partial x_{wi} / \partial y_{wi})^2 dy_{wi} = \frac{\pi^2 X_{wi}^2}{4L_i} \end{aligned} \tag{15}$$

Finally, the total tension  $T_i$  of the  $i$ th cable can be written as:

$$T_i = T_{0i} + k_{wi} \left( \Delta L_i + \frac{\pi^2 X_{wi}^2}{4L_i} \right) \tag{16}$$

where  $k_{wi}$  is the stiffness coefficient of the cable. As can be seen from Eq. (16), cable tension  $T_i$  varies with the motion of the end-effector and vibration of the cable.

### 3.2.3. Vibration equation of the cable

Based on the analysis above, considering the cable damping, the transverse vibration equation of the  $i$ th cable can be described as:

$$\ddot{X}_{wi} + c_{wi} \dot{X}_{wi} + \left( \frac{\pi}{L_i} \right)^2 \left( \frac{T_i}{\rho_w A} - v_{yi}^2 \right) X_{wi} = 0 \tag{17}$$

where cable tension  $T_i = T_{0i} + k_{wi} \left( \Delta L_i + \frac{\pi^2 X_{wi}^2}{4L_i} \right)$ ,  $v_{yi} = u_i^T \dot{X}_p + (r_i \times u_i)^T \omega$ ,  $c_{wi}$  is the damping coefficient.

### 3.3. Dynamic equation of CDPRs

Combining Eq. (2) and Eq. (17), and writing in matrix form leads to:

$$\begin{cases} \ddot{X}_w + C_w \dot{X}_w + K_w X_w = 0 \\ M \ddot{X} + W_C - W_G = J_A^T T \end{cases} \tag{18}$$



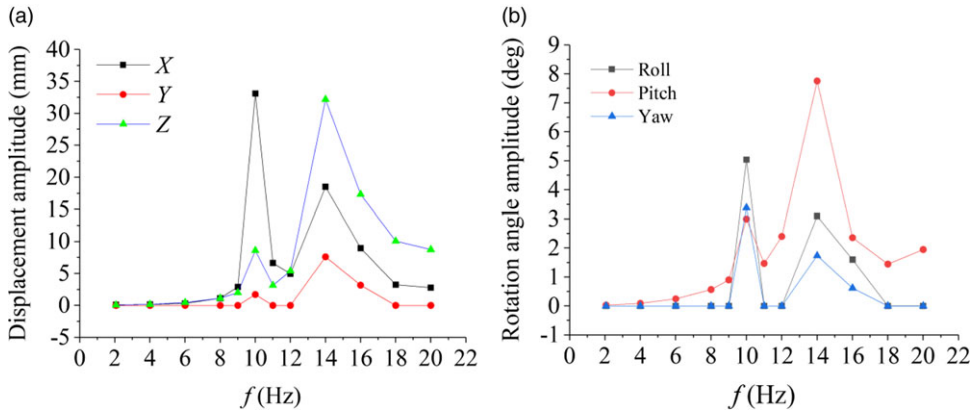


**Figure 4.** Attitude amplitude of the end-effector: (a) displacement amplitude and (b) rotation angle amplitude.

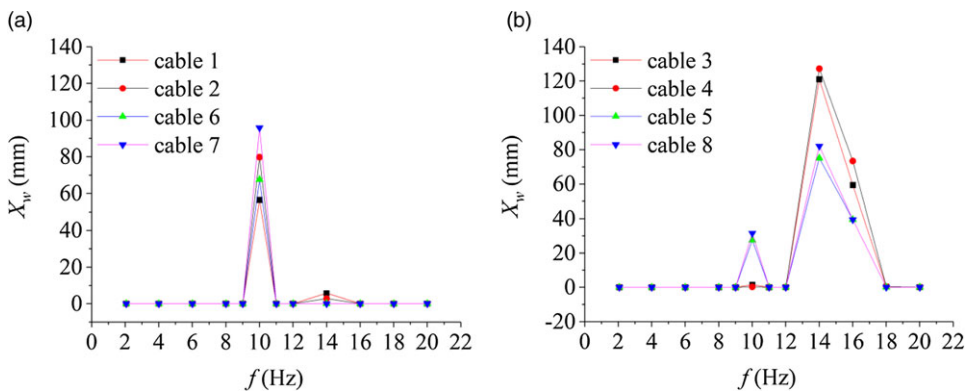


**Figure 5.** Cable amplitude: (a) cable 1, cable 2, cable 6, and cable 7, (b) cable 3, cable 4, cable 5, and cable 8.

Note that  $X_{w0i}$  is the initial deflection at the mid-span of the  $i$ th cable ( $i = 1, 2, \dots, 8$ ) perpendicular to its axis (Fig. 2), and  $X_{p0}$  is the initial disturbance of the end-effector along the direction of  $OX$ . With the initial disturbance of  $X_{p0} = 0.1$  mm and  $X_{w0i} = 0.1$  mm ( $i = 1, 2, \dots, 8$ ), Eq. (19) is solved using MATLAB with a time step of  $10^{-4}$  s.

One can assume that the motion of the end-effector is a pitching oscillation:  $\theta = A^* \sin(2\pi ft)$ ,  $A^* = 2^\circ$ . The variation interval of oscillation frequency  $f$  falls in [2.06, 20] Hz. The vibration of the cables excited by the oscillation of the end-effector and the resulting dynamic response of the CDPR are investigated.

#### 4.2. Simulation results and discussions

The frequency–amplitude relationship of the CDPR is demonstrated in Figs. 4 and 5. As shown in Figs. 4 and 5, the attitude amplitude variations of the end-effector are consistent with the cables. When the pitching oscillation frequency of the end-effector  $f < 8$  Hz, the displacement amplitudes of the end-effector are less than 0.5 mm, the rotation angle amplitudes are less than  $0.3^\circ$ , and the cable amplitudes are only 0.1 mm. It can be seen that the CDPR is stable in the frequency interval of  $f < 8$  Hz. When  $f > 8$  Hz, both the end-effector and the cables begin to occur large vibration. Especially, at the pitching oscillation frequency of  $f = 10$  Hz and  $f = 14$  Hz, the amplitudes of both the end-effector and the cables reach the maximum. At  $f = 10$  Hz, the maximum displacement amplitude of the end-effector is up to 33.10 mm,



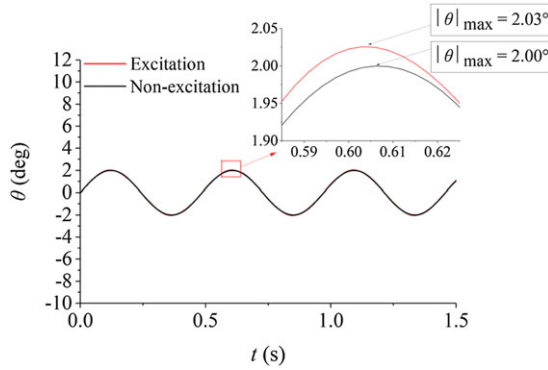


Figure 6. Pitching angle variation of the end-effector:  $f = 2.06$  Hz.

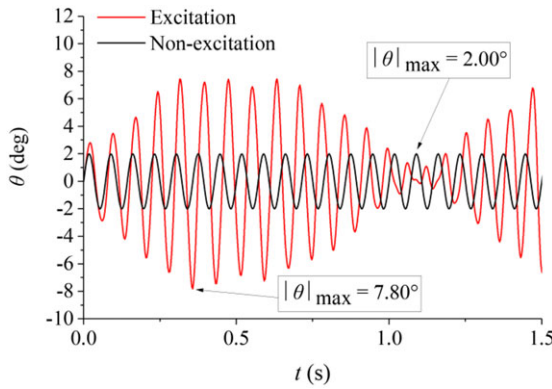


Figure 7. Pitching angle variation of the end-effector:  $f = 14$  Hz.

the maximum rotation angle amplitude is  $5.04^\circ$ , and the maximum cable amplitude is 95.87 mm. At  $f = 14$  Hz, the maximum displacement amplitude of the end-effector is up to 32.19 mm, the maximum rotation angle amplitude is  $7.76^\circ$ , and the maximum cable amplitude is 127.30 mm. Consequently, two peaks can be found at  $f = 10$  Hz and  $f = 14$  Hz, according to Figs. 4 and 5. It can be seen that the CDPR is unstable when  $f > 8$  Hz.

According to Figs. 4 and 5, it can be seen that obvious deviations in the attitude of the end-effector are caused by the vibrations of the cables and the end-effector, when the frequency is higher than 8 Hz. Therefore, it can be inferred that the reliable motion frequency for the CDPR is within 8 Hz. When the frequency is higher than 8 Hz, the influence of the flexible cables on the attitude deviation of the end-effector cannot be ignored. The flexibility of the cables needs to be considered in the motion control of the CDPR.

Besides, as shown in Figs. 4 and 5, it turns out that, as the oscillation frequency of the end-effector increases, the end-effector and the cables exhibit the dynamics process from steady state to unstable large-amplitude vibration and finally to stable small-amplitude vibration.

In order to further discuss the significance of the excitation effect caused by the axially moving length-variable cables, the results with and without excitation effect are compared. Equation (18) represents the case with excitation effect. In the case without excitation effect, we set  $X_w = 0$  in Eq. (18), that is, the cable vibration and its excitation effect on the end-effector are not considered.

As shown in Fig. 6, when the pitching oscillation frequency  $f = 2.06$  Hz, the pitching angle amplitude  $|\theta|_{\max}$  without excitation effect is  $2.00^\circ$ , while  $|\theta|_{\max}$  with excitation effect is  $2.03^\circ$ . The relative increment is only 1.5% when  $f = 2.06$  Hz. As shown in Fig. 7, when  $f = 14$  Hz, the pitching angle amplitude

**Table II.** The results of the CDPR with and without excitation effect.

Results	$f$	Non-excitation	Excitation	Relative increment (%)
$ \theta _{\max}$	2.06 Hz	2.00°	2.03°	1.5%
	14 Hz	2.00°	7.80°	290%

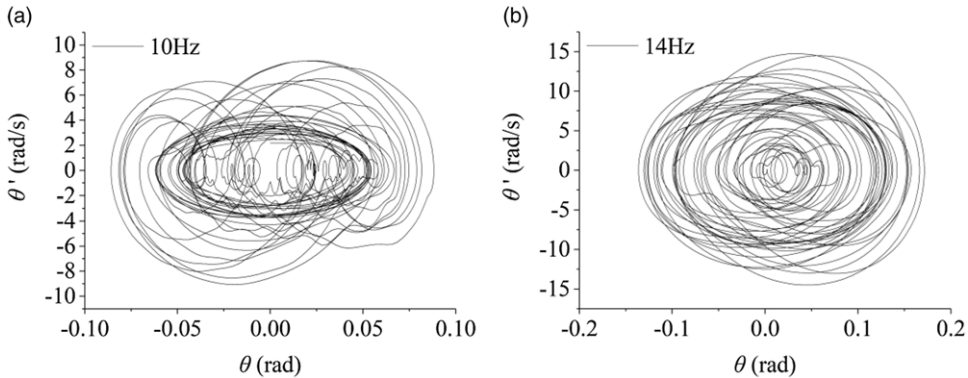


**Figure 8.** Phase diagram of pitching angle variation of the end-effector: (a)  $f = 10$  Hz, (b)  $f = 14$  Hz.

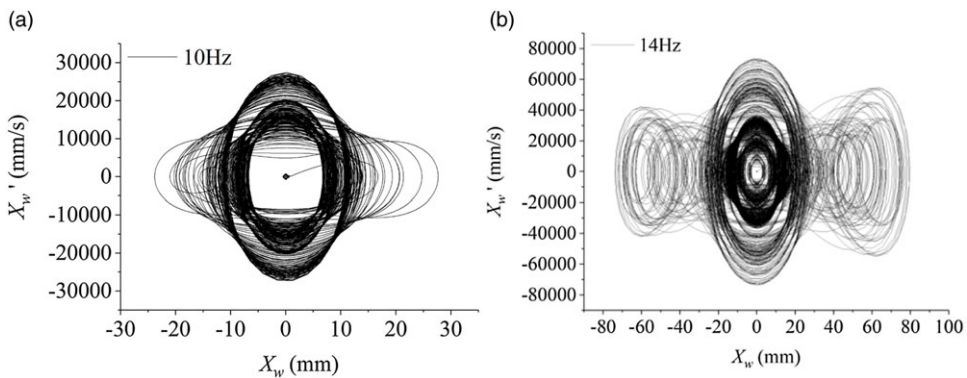


**Figure 9.** Phase diagram of the cable (cable 5): (a)  $f = 10$  Hz, (b)  $f = 14$  Hz.

$|\theta|_{\max}$  without excitation effect is 2.00°, while  $|\theta|_{\max}$  with excitation effect is 7.80°. The relative increment is 290% when  $f = 14$  Hz. The resulting data are shown in Table II.

By comparing the results with and without excitation effect of the axially moving length-variable cables at different frequencies, it can be concluded that the excitation effect can cause large attitude deviations of the end-effector in some specific frequencies  $f$ . The large attitude deviation of the end-effector can reduce the positioning accuracy of the CDPR. The proposed dynamic model of the CDPR can be used to analyze the response of the end-effector, so as to evaluate the influence of excitation effect on the attitude accuracy of the CDPR, which is of great importance.

Moreover, the phase diagrams of vibrations of the end-effector and the cables at the frequency of 10 Hz and 14 Hz are shown in Figs. 8 and 9. The pitching angle of the end-effector and the amplitude of cable 5 are taken as examples. It can be seen that both the end-effector and the cables occur large vibrations at the frequency of 10 Hz and 14 Hz, and the vibrations are non-linear. This indicates that the dynamics of the CDPR exhibit non-linear characteristics, due to the influence of flexible cables.

It can be concluded that attitude deviation of the end-effector is caused by the cable flexibility. This effect is particularly significant when the motion frequency of the end-effector is in some specific

$$\mathbf{X} = [\mathbf{0}_{1 \times 3}, 0, 2\sin(2 \times 2.06\pi t), 0]^T$$

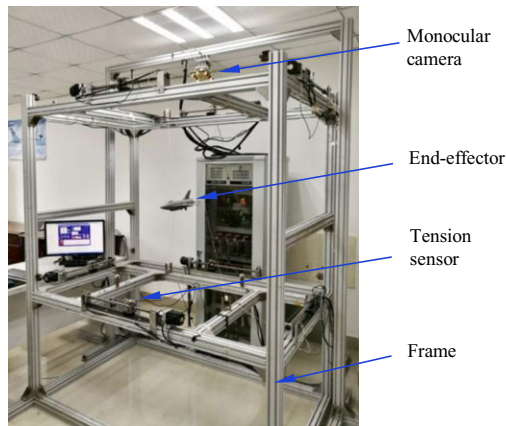


**Figure 10.** CDPR-8 prototype in lab.

intervals. With the proposed nonlinear dynamic model of the CDPRs, these intervals can be quickly identified. It would be very useful for the design of the CDPRs.

## 5. Experimental verification

Verification of the dynamic model of compliant CDPRs presented in this paper was performed in the laboratory using a 6-DOF cable-driven robot, called CDPR-8, as shown in Fig. 10. The attitude variation of the end-effector was recorded by an external monocular camera system (DH-HV1300FM CMOS, sampling frequency of 16 fps) [46]. Meanwhile, the tension in each cable was measured by the tension sensor (HBM U9C, sensitivity of 1 mV/V) connected to the end of each cable. The amplitude of the cable was not measured in the test, which was limited by the experimental equipment for such a thin cable. Thus, the cable tensions were measured to reflect the vibration of the cables.

Due to the low sampling frequency of the monocular camera system, and the limitation of the rigid-body frequency of the frame itself, only the low-frequency test was done. The test was performed considering a motion of the end-effector as follows:

$$\mathbf{X} = [\mathbf{0}_{1 \times 3}, 0, 2 \sin(2 \times 2.06\pi t), 0]^T \quad (20)$$

In the pitching oscillation test, compared to the pitching angle, the values of the other attitudes of the end-effector are very small. So only the pitching angle is concerned here. As shown in Fig. 11, the numerical and experimental values of the pitching angle amplitudes are  $2.03^\circ$  and  $1.92^\circ$ , respectively. The deviation of the numerical value from the experimental value is  $0.11^\circ$ , and the relative error is 5.73%. It turns out that the numerical results of the pitching motion match well with the experimental results. Therefore, the proposed dynamic model of compliant CDPRs is validated.

Besides, it can be seen that the experimental value of the pitching angle amplitude is slightly smaller than the numerical value. This may be due to the limited sampling frequency of the monocular camera. As shown in Fig. 11, there are nine sampling points per period. So the sampling frequency of 16 fps is only adequate for this test with the oscillation frequency  $f = 2.06$  Hz.

Cable 1 and cable 7 are taken as examples. The cable tension variation  $\Delta T_i$  is obtained by subtracting the initial cable tension  $T_{0i}$  from the instantaneous cable tension  $T_i$ . Briefly, it can be expressed as  $\Delta T_i = T_i - T_{0i}$ . The stiffness coefficients of the cables used in the simulation are obtained from the cable tension data in the low-frequency oscillation test, which are  $k_w = [1410, 1410, 1580, 1580, 1560, 1100, 1100, 1560]$  N/m.

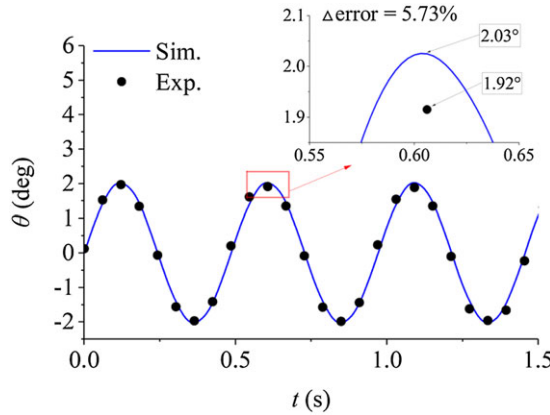


Figure 11. Pitching angle variation of the end-effector ( $f = 2.06$  Hz).

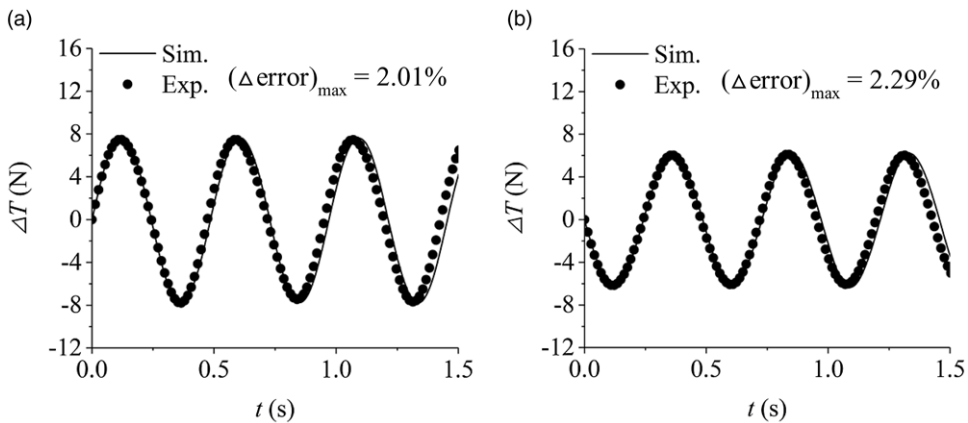


Figure 12. Cable tension: (a) cable 1 and (b) cable 7.

As shown in Fig. 12(a), the maximal tension variations of cable 1 in numerical simulation and experiment are 7.61 N and 7.46 N, respectively. The relative error between the numerical and experimental results is 2.01%. As shown in Fig. 12(b), the maximal tension variations of cable 7 in numerical simulation and experiment are 6.25 N and 6.11 N, respectively. The relative error between the numerical and experimental results is 2.29%. This shows that the difference between the maximal cable tension variations obtained by numerical simulation and experiment does not exceed 0.15 N, and the relative error is not more than 2.29%. It means that the numerical results of the cable tension variation are consistent with the experimental values, which validates the proposed dynamic model of compliant CDPRs.

In addition, it can be found that the frequencies of the cable tension variation obtained from the experiment and simulation do not match very well. Some factors are not considered in the simulation, such as the friction between the cable and the pulley, and the hysteresis effect of the cable. This may be the reason for the minor inconsistency on the frequencies of the cable tension variation between the simulation and experiment.

### 6. Conclusions

With the intention to characterize the dynamic behaviors of compliant CDPRs containing flexible cables, this paper focuses on both the vibration of axially moving length-variable cable and the reaction of the

vibrating cables on the end-effector. A model for transverse vibration of the axially moving length-variable cable is developed. Then, an original nonlinear dynamic model of CDPRs able to capture the vibration of the cables and the dynamics of the end-effector is proposed. Based upon the proposed model of a 6-DOF 8-cable CDPR, the frequency–amplitude relationship of the CDPR is obtained. Moreover, the significance of the excitation effect caused by the axially moving length-variable cables is demonstrated by comparing the results with and without excitation effect at different frequencies. It is proved that the oscillation of the end-effector can cause vibration in the cables, and the vibrating cables can react on the end-effector causing large-amplitude vibration both in the end-effector and the cables. It turns out that, as the oscillation frequency of the end-effector increases, the end-effector and the cables exhibit the dynamics process from steady state to unstable large-amplitude vibration and finally to stable small-amplitude vibration. This indicates that the dynamics of the CDPR exhibit non-linear characteristics, due to the influence of flexible cables. In the frequency interval where large-amplitude vibration of the CDPR occurs, the influence of the flexible cables on the attitude deviation of the end-effector cannot be ignored. The proposed dynamic model of compliant CDPRs is validated by experiments performed in the laboratory using a 6-DOF cable-driven robot, called CDPR-8. This work provides an effective methodology for the dynamic analysis of CDPRs. Research on the dynamics of CDPRs can provide constructive guidelines for the design, motion control, and optimization of CDPRs.

Besides, due to the complex characteristics of the damping of the Kevlar cable, such as nonlinearity, viscoelasticity, and hysteretic, the modeling of the cable damping is simplified in this paper. In future research, the damping force of the cable will be further studied.

**Author contributions.** Guowu Wei and Qi Lin conceived and designed the study. Miaoqiao Peng performed the simulations. Longhai Xiao and Miaoqiao Peng conducted the experiments. Jiayong Zhuo collected the simulation results. Miaoqiao Peng, Longhai Xiao, and Qinglin Chen wrote the article.

**Financial support.** This work was supported by the National Natural Science Foundation of China (51909103, 11702232), Natural Science Foundation of the Fujian Province of China (2021J05164), Foundation of education department of the Fujian Province of China (JAT200267), the Scientific Research Foundation of Jimei University of China (ZQ2020022), and Foreign Cooperation Project of Department of Science and Technology of Fujian Province (2022I0019).

**Competing interests.** The authors declare that they have no Competing interest.

## References

- [1] X. G. Wang and Q. Lin, “Advances of cable-driven parallel suspension technologies in wind tunnel tests,” *Acta Aeronaut. Astronaut. Sin.* **39**(9), 022064 (2018) (in Chinese).
- [2] M. Rognant and E. Courteille, “Improvement of Cable Tension Observability through a New Cable Driving Unit Design,” **In: Cable-Driven Parallel Robots 2018: Mechanisms Machine Science, The Third International Conference on Cable-Driven Parallel Robots**, vol. 53 (Springer, Cham, 2018) pp. 208–291.
- [3] Y. Su, Y. Y. Qiu and P. Liu, “Optimal cable tension distribution of the high-speed redundant driven camera robots considering cable sag and inertia effects,” *Adv. Mech. Eng.* **6**(2014), 729020 (2014).
- [4] H. L. Wei, Y. Y. Qiu and Y. Sheng, “On the cable pseudo-drag problem of cable-driven parallel camera robots at high speeds,” *Robotica* **37**(10), 1695–1709 (2019).
- [5] G. Rosati, P. Gallina and S. Masiero, “Design, implementation and clinical tests of a Cable-based robot for neurorehabilitation,” *IEEE Trans. Neural Syst. Rehabil. Eng.* **15**(4), 560–569 (2007).
- [6] Y. L. Wang, K. Y. Wang, Y. J. Chai, Z. J. Mo and K. C. Wang, “Research on mechanical optimization methods of cable-driven lower limb rehabilitation robot,” *Robotica* **40**(1), 154–169 (2022).
- [7] P. Lafourcade, M. Libre and C. Reboulet, “Design of a Parallel Cable-driven Manipulator for Wind Tunnels,” **In: Fundamental Issues and Future Research Directions for Parallel Mechanisms and Manipulators, The Workshop on Fundamental Issues and Future Directions for Parallel Mechanisms and Manipulators**, Quebec, Canada (2002) pp. 187–194.
- [8] M. Holden, T. Wadhams, M. MacLean, A. Dufrene and E. Marineau, “A Review of Basic Research and Development Programs Conducted in the Lens Facilities in Hypersonic Flows,” **In: AIAA 2012-0469, 50th AIAA Aerospace Sciences Meeting including the New Horizons Forum and Aerospace Exposition**, Nashville, TN, USA (2012) pp. 1–17.
- [9] Y. W. Xiao, Q. Lin, Y. Q. Zheng and B. Liang, “Model aerodynamic tests with a wire-driven parallel suspension system in low-speed wind tunnel,” *Chin. J. Aeronaut.* **23**(4), 393–400 (2010).

- [10] X. G. Wang, M. J. Peng, Z. H. Hu, Y. S. Chen and Q. Lin, "Feasibility investigation of large-scale model suspended by cable-driven parallel robot in hypersonic wind tunnel test," *Proc. Inst. Mech. Eng. G J. Aerosp. Eng.* **231**(13), 2375–2383 (2016).
- [11] B. Zi, B. Y. Duan, J. L. Du and H. Bao, "Dynamic modeling and active control of a cable-suspended parallel robot," *Mechatronics* **18**(1), 1–12 (2008).
- [12] H. Yuan, E. Courteille, M. Gouttefarde and P. E. Hervé, "Vibration analysis of cable-driven parallel robots based on the dynamic stiffness matrix method," *J. Sound Vib.* **394**, 527–544 (2017).
- [13] J. L. Du, H. Bao, C. Z. Cui and D. W. Yang, "Dynamic analysis of cable-driven parallel manipulators with time-varying cable lengths," *Finite Elem. Anal. Des.* **48**(1), 1392–1399 (2012).
- [14] X. Weber, L. Cuvillon and J. Gangloff, "Active Vibration Canceling of a Cable-Driven Parallel Robot using Reaction Wheels," **In: IEEE/RSJ International Conference on Intelligent Robots and Systems 2014, IEEE/RSJ International Conference on Intelligent Robots and Systems (IROS 2014)**, Chicago, IL, USA (2014) pp. 1724–1729.
- [15] H. Yuan, E. Courteille and D. Deblaise, "Static and dynamic stiffness analyses of cable-driven parallel robots with non-negligible cable mass and elasticity," *Mech. Mach. Theory* **85**, 64–81 (2015).
- [16] S. Kawamura, H. Kino and C. Won, "High-speed manipulation by using parallel wire-driven robots," *Robotica* **18**(1), 13–21 (2000).
- [17] M. Hassan and A. Khajepour, "Analysis of bounded cable tensions in cable-actuated parallel manipulators," *IEEE Trans. Robot.* **27**(5), 891–900 (2011).
- [18] W. Kraus, P. Miermeister and A. Pott, "Investigation of the Influence of Elastic Cables on the Force Distribution of a Parallel Cable-Driven Robot," **In: Cable-Driven Parallel Robots 2013: Mechanisms and Machine Science, International Conference on Cable-Driven Parallel Robots**, vol. 12 (Springer, Berlin, 2013) pp. 103–115.
- [19] T. Rasheed, P. Long, D. Marquezgamez and S. Caro, "Tension Distribution Algorithm for Planar Mobile Cable-Driven Parallel Robots," **In: Cable-Driven Parallel Robots 2018: Mechanisms Machine Science, The Third International Conference on Cable-Driven Parallel Robots**, vol. 53 (Springer, Cham, 2018) pp. 268–279.
- [20] S. Perreault, P. Cardou, C. Gosselin and J. Otis, "Geometric determination of the interference-free constant-orientation workspace of parallel cable-driven mechanisms," *J. Mech. Robot.* **2**(3), 031016 (2010).
- [21] A. Berti, J. P. Merlet and M. Carricato, "Solving the direct geometrico-static problem of underconstrained cable-driven parallel robots by interval analysis," *Int. J. Robot. Res.* **35**(6), 723–739 (2016).
- [22] X. Jiang and C. Gosselin, "Dynamic point-to-point trajectory planning of a three-DOF cable-suspended parallel robot," *IEEE Trans. Robot.* **32**(6), 1550–1557 (2016).
- [23] N. Zhang and W. Shang, "Dynamic trajectory planning of a 3-DOF under-constrained cable-driven parallel robot," *Mech. Mach. Theory* **98**, 21–35 (2016).
- [24] M. A. Khosravi and H. D. Taghirad, "Dynamic analysis and control of cable driven robots with elastic cables," *Trans. Can. Soc. Mech. Eng.* **35**(4), 543–557 (2011).
- [25] R. Chellal, L. Cuvillon and E. Laroche, "Model identification and vision-based  $H_{\infty}$  position control of 6-DOF cable-driven," *Int. J. Control* **90**(4), 684–701 (2017).
- [26] Y. Zhang, S. K. Agrawal and M. J. Piovoso, "Coupled Dynamics of Flexible Cables and Rigid End-effector for a Cable Suspended Robot," **In: 2006 American Control Conference**, Minneapolis, MN, USA (2006) pp. 3880–3885.
- [27] X. M. Diao and O. Ma, "Vibration analysis of cable-driven parallel manipulators," *Multibody Syst. Dyn.* **21**(4), 347–360 (2009).
- [28] K. Lin, D. J. Zou and M. H. Wei, "Nonlinear analysis of cable vibration of a multispan cable-stayed bridge under transverse excitation," *Math. Probl. Eng.* **2014**, 1–13 (2014).
- [29] E. M. Mockensturm and J. P. Guo, "Nonlinear vibration of parametrically excited, viscoelastic, axially moving strings," *J. Appl. Mech. Trans. ASME* **72**(3), 374–380 (2005).
- [30] M. Lepidi and V. Gattulli, "A parametric multi-body section model for modal interactions of cable-supported bridges," *J. Sound Vib.* **333**(19), 4579–4596 (2014).
- [31] G. Tagata, "Harmonically forced, finite amplitude vibration of a string," *J. Sound Vib.* **51**(4), 483–492 (1977).
- [32] J. H. G. Macdonald, "Multi-modal vibration amplitudes of taut inclined cables due to direct and/or parametric excitation," *J. Sound Vib.* **363**, 473–494 (2016).
- [33] V. V. Tzanov, B. Krauskopf and S. A. Neild, "Vibration dynamics of an inclined cable excited near its second natural frequency," *Int. J. Bifurcat. Chaos* **24**(9), 1430024 (2014).
- [34] M. Lepidi and V. Gattulli, "Non-linear interactions in the flexible multi-body dynamics of cable-supported bridge cross-sections," *Int. J. Nonlinear Mech.* **80**, 14–28 (2016).
- [35] M. Demšić, M. Uroš, A. J. Lazarević and D. Lazarevi, "Resonance regions due to interaction of forced and parametric vibration of a parabolic cable," *J. Sound Vib.* **447**, 78–104 (2019).
- [36] L. Q. Chen, Y. Q. Tang and J. W. Zu, "Nonlinear transverse vibration of axially accelerating strings with exact internal resonances and longitudinally varying tensions," *Nonlinear Dyn.* **76**(2), 1443–1468 (2014).
- [37] A. H. Nayfeh and D. T. Mook. *Nonlinear Oscillations* (Wiley, New York, 1979).
- [38] C. D. Mote, "On the nonlinear oscillation of an axially moving string," *J. Appl. Mech.* **33**(2), 463–464 (1966).
- [39] M. H. Ghayesh, "Stability characteristics of an axially accelerating string supported by an elastic foundation," *Mech. Mach. Theory* **44**(10), 1964–1979 (2009).
- [40] M. H. Ghayesh, "Parametric vibrations and stability of an axially accelerating string guided by a non-linear elastic foundation," *Int. J. Nonlinear Mech.* **45**(4), 382–394 (2010).



- [41] A. Yurddaş, E. Özkaya and H. Boyaci, “Nonlinear vibrations of axially moving multi-supported strings having non-ideal support conditions,” *Nonlinear Dyn.* **73**(3), 1223–1244 (2013).
- [42] A. Yurddaş, E. Özkaya and H. Boyaci, “Nonlinear vibrations and stability analysis of axially moving strings having nonideal mid-support conditions,” *J. Vib. Control* **20**(4), 518–534 (2014).
- [43] R. A. Malookani and W. T. van Horssen, “On parametric stability of a nonconstant axially moving string near resonances,” *J. Vib. Acoust.* **139**(1), 011005 (2017).
- [44] M. J. Peng, H. S. Wu, Q. Lin, F. G. Zhou, T. Liu and X. G. Wang, “Dynamic characteristics of wire-driven parallel robot with wire damping,” *J. Beijing Univ. Aeronaut. Astronaut.* **46**(2), 304–313 (2020) (in Chinese).
- [45] H. M. Irvine and T. K. Caughey, “The linear theory of free vibrations of a suspended cable,” *Proc. R. Soc.* **341**(1626), 299–315 (1974).
- [46] Y. F. Ji, Q. Lin, Z. H. Hu, M. J. Peng and Y. Q. Wang, “Feasibility investigation on dynamic stability derivatives test of SDM model with wire-driven parallel robot suspension system,” *Acta Aeronaut. Astronaut. Sin.* **39**(1), 121330 (2018) (in Chinese).